Path Planning Under MIMO Network Constraints for Throughput Enhancement in Multi-robot Data Aggregation Tasks

Alexandra Pogue[1], Samer Hanna[2], Andy Nichols[3], Xin Chen[4], Danijela Cabric[2], and Ankur Mehta[2]

Abstract— Under line-of-sight (LOS) network conditions, multi-input multi-output (MIMO) wireless communications can increase the channel capacity between a team of robots and a multi-antenna array at a stationary base station. This increased capacity can result in greater data throughput, shortening the time necessary to complete channel-limited data aggregation tasks. To take advantage of this higher capacity channel, the robots in the team must be positioned to maximize complex channel orthogonality between each robot and receiver antenna. Using geometrically motivated assumptions, we derive transmitter spacing rules that can be easily be added on to existing path plans to improve backhaul throughput for data offloading from the robot team, with minimal impact on other system objectives. We demonstrate the effectiveness of the approach— both in ideal as well as realistic channels outside the domain of our simplifying assumptions—with numerical examples of robot-coordinated path plans in two example environments, achieving up to 42% improvement in task completion times.

I. INTRODUCTION

In recent years there has been considerable focus on deployment of multi-robot teams for cooperative field missions [1]. To work around issues of intermittent connectivity and limited communication bandwidth robots must operate autonomously when disconnected, periodically seeking the location of high-strength communication links to transmit collected data and receive updates from the base station [2]–[8]. This limits the ability for continuous data streaming throughout a sensing task. Real-time streaming is particularly necessary in applications where autonomous operation is currently unsolved or would require more computation than is reasonable to carry on the robots, such as in tracking and surveillance or human-driven inspection tasks. Other applications, in particular search and rescue missions, may also require real-time streaming due to the time critical immediacy of the underlying objective. Several approaches to maintaining connectivity for all time are possible; many relevant robotics works in path planning, however, pose sensing and capacity as a multi-objective optimization problem subject to a static channel map [9], [10].
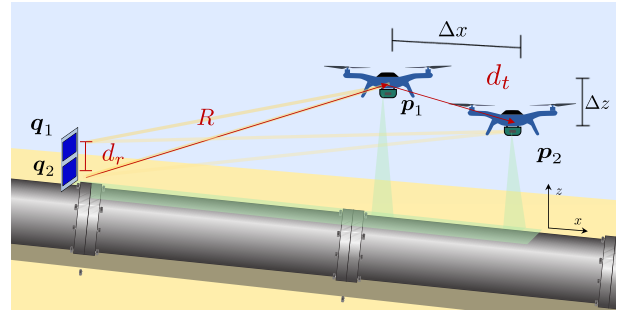
(a) When sensing data is distributed along one dimension, transmitters can change their altitude to generate separation Δz to improve communication capacity.
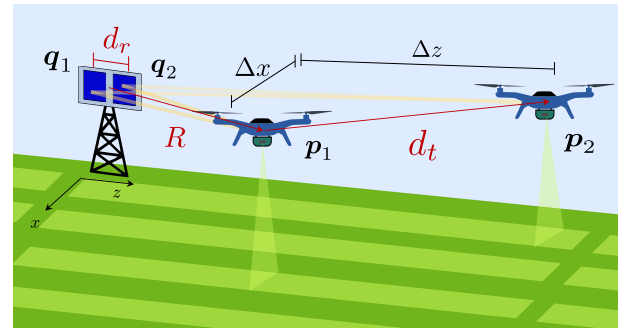
(b) When sensing data is distributed along two dimensions, transmitters maintain a fixed altitude and travel with separation Δz within the horizontal plane to improve communication capacity.

Fig. 1: Two example scenarios of a multi-receiver, multi-transmitter system where communication-aware techniques are applied to improve transmission throughput in time-critical sensing missions.

In this paper, we employ spatial multiplexing (SM), a distributed multi-input multi-output (MIMO) communication technique [11]–[13]. The SM communication system attempts to increase the communication capacity (i.e. data throughput) by using multiple transmit and receive antennas to send unique data streams simultaneously. SM is typically used in cluttered (or rich scattering) environments because independent fading aids in decoding signals at the receiver. SM can provide throughput gains in line-of-sight (LOS) environments as well, but requires care in placement of antennas in addition to typical signal processing for decoding streams [14]–[17]. Work has been done to create virtual antenna arrays using unmanned aerial vehicles (UAVs) as dedicated network enhancers for signal relay applications, among others [18]–[21]. In this work we use the same

principles given in [14]–[17] to create *mobile* virtual arrays capable of coordination within a cluster to enhance network link quality while simultaneously moving and collecting data.

SM can significantly enhance the quality of network links subject to path loss to facilitate improved real-time data aggregation in LOS-dominant areas, i.e. areas where other causes of intermittent signals such as shadowing or multipath fading are not pronounced. In this work we mitigate data stream correlation caused by interference among robots by positioning transmitters such that communication channels have an optimized phase offset. We do so by constraining robot transmitters to uniform linear arrays (ULA) [14], [15]. In largely unobstructed areas, boustrophedon flight plans are the standard for aerial coverage missions [22], [23]. In this work we show the flight planner can enjoy significant capacity gains by integration of ULA configurations into pre-existing boustrophedon plans, with little effort in adoption. Futhermore, our ULA adaptation ensures that the ground coverage of the sensing field of view is a superset of the coverage set of the prior unmodified trajectories.

Fig. 1 shows an example of two situations where ULA adaptation is used to increase communication throughput. Robots maintain an inter-transmitter distance, d_t, for a total distance of $(m - 1) \cdot d_t$ from the 1st to the mth robot in the direction $\vec{d_t}$, where M is the total number of robot transmitters. Inter-transmitter distance changes with respect to the x-coordinate of the 1st robot. In Fig. 1a robots adjust the altitude differential prescribed by d_t as they collect data along a path. This configuration captures applications such as powerline [24]–[27], bridge [28]–[32], and pipeline infrastructure inspection [33]–[35]. In Fig. 1b robots maintain constant altitude while d_t changes within the horizontal plane containing the receiver antennas. This approach is appropriate for applications requiring real-time transmission in coverage missions such as search and rescue [10], [36] and surveillance [37]–[39].

A. Motivating Example

In remote missions with MIMO wireless infrastructure, robot teams may sacrifice available throughput via naïve positioning. In a UAV coverage mission, there are several boustrophedon possibilities; considering various options can mitigate interference and make a substantial difference in the rate of data transmission.

Using the communication model given in Sec. II-B, we create the example depicted in Fig. 2 where UAVs sweep an area of interest without a particular spatio-temporal objective, such as in the monitoring of a forest fire. The UAV transmitters in scenario (a) are subject to nearly identical (highly correlated) SM channels due to poor positioning. UAVs achieve an average communication capacity of 2.41 bps/Hz and 1.51 bps/Hz for the closer and more remote transmitters respectively. In scenario (b) the UAVs reorient with respect to receivers. Here both transmitters achieve approximately the same average capacity of 7.08 bps/Hz. This means that on average they can transmit 3.6 times the data over the same time interval.
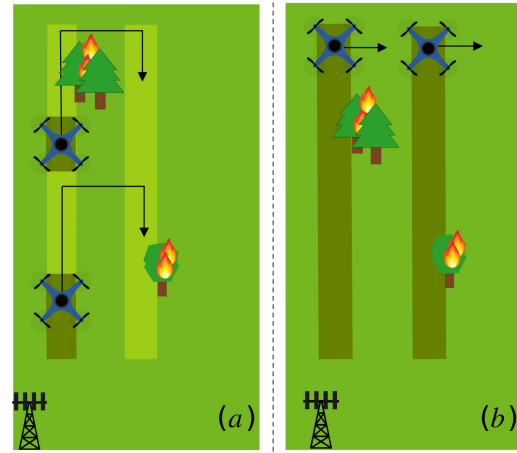

Fig. 2: Two possible paths transmitters may take without changing the mission objective. Black arrows indicate direction of travel. The robots traverse the dark green paths in 1 hour. Because robots minimize interference in (b), they travel much farther.

Assuming we always meet sensing requirements, we motivate our work using time as a performance metric. For a clear side-by-side comparison of MIMO methods, we enforce the even distribution of data over a spanned area. Transmitter velocity is defined as a function of available capacity: transmitters may only move as fast as the rate at which they can transmit data in real-time. Reassessing the previous example, the dark green colored portion of paths represent the sensing area covered by UAVs in 1 hour. In scenario (a) the UAVs collectively cover 554 m of ground while in scenario (b) the UAVs cover 2 km. It is clear then that scenario (b) is preferable, and at no cost to the sensing objective.

B. Contributions

In this paper we develop the integration of ULA formations with flight plans for real-time data aggregation tasks. To the best of the authors' knowledge, this is the first work to incorporate SM MIMO approaches based on the analysis of complex communication signals into a mobile, simultaneous sensing and transmitting multi-robot system. This research characterizes the advantages of LOS SM approaches as as tool for communications enhancement, and serves as a foundation for solving SM-aware path plans for sophisticated sensing objectives. Results showing up to a 42% improvement in task completion times in analytical examples and 29% in realistic simulation further demonstrate the effectiveness of this research.

II. PROBLEM SETUP

M robots are simultaneously sending independent data streams using SM communications to N fixed ground receivers, where $N \geq M$. We examine two tasks where behavior is constrained to an in-plane Cartesian workspace $\mathcal{W} \subset \mathbb{R}^2$. In all cases, robot velocity is throttled by available capacity in the "sensing direction". In the one-dimensional

(1D) case robots travel in series, and collect data along a line. Robots may change altitude at any velocity, but may not move along their sensing path faster than they can transmit data. In the 2D scenario data is distributed in two directions; robots are only sensing, however, when traveling along the boustrophedon path.

A. Motion Model

At time instant t, the mth transmitter is located at $p_m(t)$ and the nth receiver is located at q_n. Mobile transmitter motion is defined by a first-order, discrete-time, kinematic model, $p_{m_{i+1}} = p_{m_i} + v_{m_i} dt_i$, where p_m, $v_m \in \mathbb{R}^2$ are the transmitter position and velocity for transmitter m respectively. The propagation time from state i to $i+1$ is the scalar value dt_i. All solutions are found using a grid-based approach consisting of equally spaced waypoints.

B. Communication Model

We derive our model based on perfect knowledge of a path LOS-dominant channel, an approximation suitable for open spaces with minimal obstruction. When a transmitter sends the data symbols $x \in \mathbb{C}^M$, the received symbols will be as follows

$$\mathbf{y} = \mathbf{H}x + \mathbf{n} \tag{1}$$

where $\mathbf{H} \in \mathbb{C}^{N \times M}$ is the channel matrix, and $[\mathbf{H}]_{n,m}$ represents the channel between the mth transmitter and the nth receiver. $\mathbf{n} \in \mathbb{C}^N$ is a Gaussian random variable modeling the additive white Gaussian noise.

One way to measure the amount of information that can be sent over a communication channel is the capacity. For a MIMO channel, the capacity is given by

$$C = \log \left(\det \left(\mathbf{I} + \rho \mathbf{H}^H \mathbf{H} \right) \right), \tag{2}$$

where ρ is the signal-to-noise-ratio of the signal.

Our focus in this paper is on scenarios that occur in an open environment, where the communication channel is assumed to be dominated by the line-of-sight (LOS) component. The elements of the channel matrix in that case can be modeled using

$$h_{n,m} = [\mathbf{H}]_{n,m} = \frac{\lambda}{4\pi \|p_m - q_n\|} \exp \left(j \frac{-2\pi \|p_m - q_n\|}{\lambda} \right) \tag{3}$$

where $\|p_m - q_n\|$ is the distance between the transmitter and the receiver and λ is the wavelength.

The transmitters are assumed to be sending independent data streams. Each transmitter does not have the data of the other transmitter, hence, all the processing has to be done at the receiver. At the receiver side, we assume that linear minimum-mean-squared-error MMSE combining is used. When using MMSE combining, the maximum rate obtained by the mth stream is given by [13]

$$C_m = \log \left(1 + P_m \mathbf{h}_m^H \left(N_0 \mathbf{I} + \sum_{i \neq m}^{M} P_i \mathbf{h}_i \mathbf{h}_i^H \right)^{-1} \mathbf{h}_m \right) \tag{4}$$

where P_m is the transmit power of the mth transmitter, N_0 is the noise power spectral density, $\mathbf{h}_m$ is the mth column of $\mathbf{H}$, and $(\cdot)^H$ denotes the Hermitian transpose. In this analysis we assume that all transmitters have the same power P, i.e, $P_m = P$ for all m.

III. EFFECTS OF TRANSMITTER POSITION ON THE MIMO NETWORK

In the LOS environment, changing path length with respect to receivers effects the channel and capacity according to (3), (4) respectively. If robots are transmitting far away from receivers, small displacements have little impact on channel magnitude, which can be approximated by $\|h_{m,n}\| \approx \frac{\lambda}{4\pi R} \ \forall \ m, n$. R in this equation approximates $d_{m,n} = \|p_m - q_n\|$ defined in (3), constraining robots to a small cluster. Under these conditions we generate uncorrelated channels by positioning robots to achieve streams with a $360° \cdot 1/M$ phase offset to a given receiver. Formally, the eigenvalues of expression $\mathbf{HH}^H$ should be nonzero to achieve a high rank LOS channel matrix and high capacity, which can be achieved by consideration of channel phase alone.

In the adaptation of path plans we use heuristics from [14], [15] to pose the communication problem as a *mobile* ULA. A ULA assumes at a given way point, robots are equally spaced. Specifically, signal orthogonality can be achieved through state-dependent phase adjustment,

$$\sum_{n=0}^{N-1} \exp \left(jn \frac{-2\pi d_r \Delta z}{\lambda R_x} \right) = 0. \tag{5}$$

This phasing relationship implies the relation,

$$\frac{d_r \Delta z}{R_x} = \frac{\lambda}{N} \tag{6}$$

between adjacent robots. The above relation generally applies when R is large, and when arrays are *parallel*, i.e. when R is equal to its projection R_x and $d_t = \Delta z$. In this research we apply (6) to scenarios outside of these constraints, but find it remains useful when constraints are relaxed.

For simplification, we analyze the capacity of transmitter 2, C_2, using the $N \times M = 2 \times 2$ case. We assess relative performance of three SM approaches to path planning using (4). In all approaches $d_r = 5$ m. Increasing d_r serves to decrease the separation Δz required to achieve a high rank H. For all parameters used to evaluate capacity, see Table I. The first of three approaches is a naïve baseline where $\Delta z = 0$ m, the second is a method with a fixed value of $\Delta z = 150$ m, and the third uses the linear relation (6). In each approach $p_1(t) = f(R(t))$ is specified by the path planner. The location of the second robot transmitter, $p_2(t)$, is then fully defined by the sensing parameter Δx and the communication parameter Δz, thus $p_2(t) = f(R(t), \Delta x, \Delta z)$.

We analyze each method in Figs. 3 and 4. From (6) we see that Δz is given by the x-position of robot 1, R_x (Fig. 3a). Fig. 3b maps C_2 as robot transmitters move along a line 20 km in the x-direction, sweeping over transmitter ground separation, $\Delta x \in [0, \ 500]$ m. The plot illustrates the effect of changing the Δx parameter on capacity in the
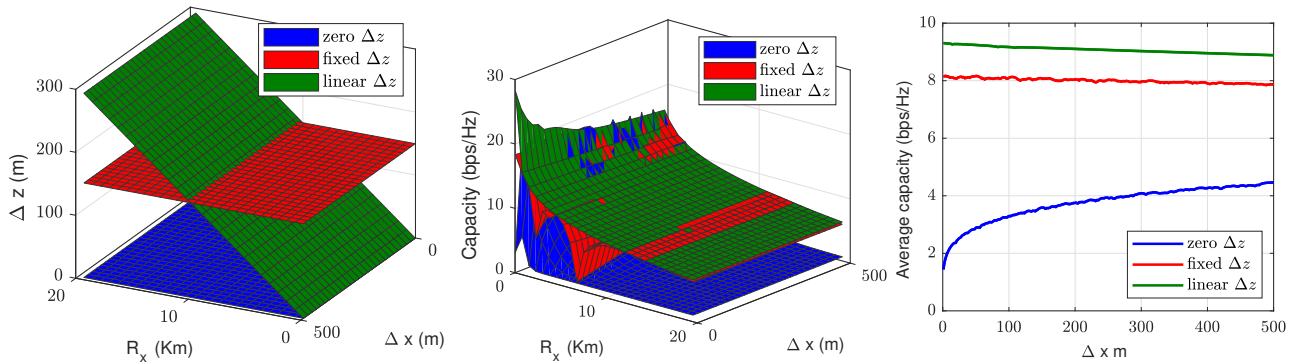
(a) Communication parameter Δz is plotted as a function of distance in the x-direction from receivers and the sensing parameter Δx. Parameter Δz varies with R_x only.

(b) Capacity is plotted as a function of distance in the x-direction from receivers and the sensing parameter Δx. Here $R_z = 0$.

(c) Plot depicting average capacity over total x-distance traveled for varying values of Δx.

Fig. 3: Plots showing the Δz and capacity calculated for 3 SM path planning approaches for a 2 transmitter, 2 receiver system where travel is in the x-direction with varying ground distance between receivers, Δx. The plot in (a) also corresponds to Fig. 4.
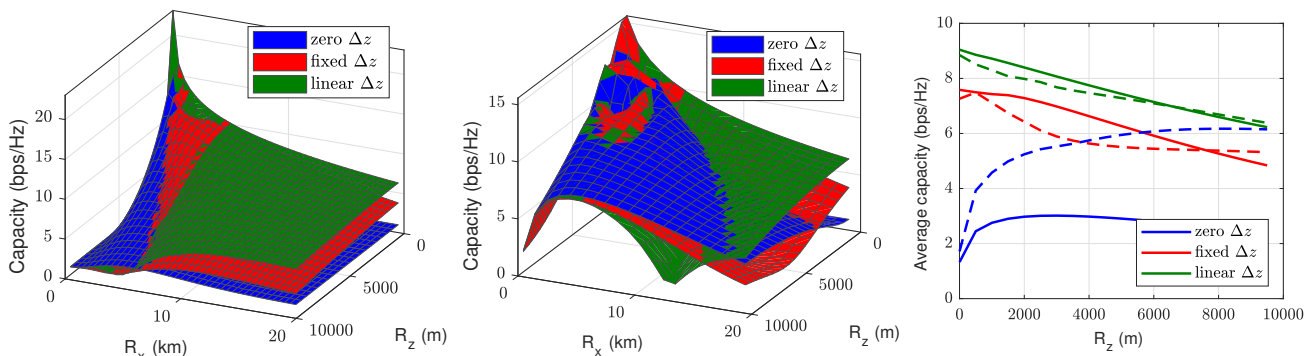
(a) Capacity is plotted for as a function of distance from receivers in the x and z-directions using a boustrophedon path plan for the value $\Delta x = 50$.

(b) Capacity is plotted for as a function of distance from receivers in the x and z-directions using a boustrophedon path plan for the value $\Delta x = 500$.

(c) Plot depicting average capacity over total x-distance traveled and lateral distance R_z from receivers.

Fig. 4: Plots showing the capacity calculated for 3 SM path planning approaches in a 2 receiver, 2 transmitter system where travel is in the x and z-directions using boustrophedon path plans of differing transmitter separation, Δx.

path following 1D scenario. Here Δx can be small if sensor redundancy is required, or UAVs performing heterogeneous sensing tasks travel in a tight cluster. Otherwise large ground separation can allow for robots to collect data independently. To better approximate a parallel array system in the 1D case, if receivers are on the ground, transmitter 1 moves at ground level, i.e. $R = R_x$. As ground distance from receivers increases, we see attenuation of capacity from path loss. We also see slight attenuation as transmitter ground separation, Δx, increases. This is expected given we are relaxing the small cluster and parallel array relations.

Figs. 4a and 4b refer to the 2D scenario, where sensing requirements generate motion in both the x and z-directions. Two values of Δx were chosen, 50 and 500 m, for the purpose of demonstrating the effect of the parallel array and small cluster relaxations. The plots illustrate the effect of motion in the z-direction that causes receiver and transmitter arrays to become "less parallel". The map is generated via the calculation of C_2 as robot transmitters move along a

boustrophedon path (see Fig. 1b). The robots move in the x-direction, R_x, by the same distance as the shown in the 1D case. They move 10 km in the z-direction, with robot 2 moving outside the sensing region of interest (ROI) to satisfy the Δz requirement (see Sec. IV for explanation). With receivers located at the origin, the plots give us information about a square 20×20 km region due to symmetry. As expected, we see the attenuation of C_2 as R becomes large. To address parallel ULA constraints, methods accounting for R_z in (6) can be applied [16].

All capacity maps demonstrate the effectiveness of the mobile ULA, or linear Δz method in mitigating interference issues in broad areas of transmitter travel. This is also demonstrated in Figs. 3c and 4c. In Fig. 3c, methods are compared based on the average capacity over the entire distance of robot travel, for each value of Δx. We see in this figure that because R_z was constrained to be zero, the more "parallel" relationship between transmitter and receiver arrays resulted in clearer performance gains. Fig. 4c shows the average

capacity value for total travel in the x-direction over the increasing interval $[0, R_z]$. The solid line corresponds to Fig. 4a and the dashed to Fig. 4b. The convergence in dashed lines as R_z increases shows the compounding effect of a large $\frac{d_t}{R}$ ratio, in addition to large R_z.

IV. MOTION PLANNING

Using the scenario from Sec. II, time is tabulated as a performance measure for different SM approaches in a 2×2 MIMO system. SM methods from the previous section are applied, and the widely adopted time-division multiple access MIMO approach (TDMA) is also included [11]. Sec. IV-A uses analytical equations given by the communication model while Sec. IV-B uses realistic channel data taken from a ray tracing simulation. Robots are constrained to move at the same velocity, and the previously defined motion model is used to calculate the total time to complete a task, $T = \sum_{i=0}^{n-1} dt_i$.

A. Motion Planning Using the LOS Equation

Temporal solutions to more specific path plans using the general concepts covered are given in this section. Simulation parameters are listed in Table I.

TABLE I: Simulation Parameters

Parameter	Definition
bandwidth	1 MHz
data density	25 Mb/m
sensing velocity	$C_2/25$ m/s
carrier frequency	1 GHz
transmission power	20 dBm
d_r	5 m
Δx	50, 150, 300, 450 m
1D R_x, R_z	$R_x \in [1, 3]$ km, $R_z = 70, 220$ m (depending on method)
2D R_x, R_z	$R_x \in [1, 3]$ km, $R_z = [0, 500]$ m
grid resolution	10 m

1) 1D Path Planning: Adjustment to 1D path plans are made using the four SM approaches– zero Δz, fixed Δz, linear Δz, and TDMA. In the first, both robots are constrained to have the same altitude. Under this constraint, empirically performance increases with an increase in altitude, $R_z = 220$ m and $\Delta z = 0$. The second maintains a fixed altitude differential, $R_z = 70$ and $\Delta z = 150$ m. The third uses the linear approach, where $R_z = 70$ m and Δz varies according to (6). Depending on the needs of the application, we assume these altitude constraints –amounting to focal distance changes in an imaging application, for example– can be accommodated. Waypoints for the TDMA approach are equivalent to the zero Δz method. The capacity for this approach is given by,

$$C_m = f_m \log \left(1 + \rho \mathbf{h}_m^H \mathbf{h}_m\right). \tag{7}$$

It assumes maximal ratio combining, f_m is the fraction of time allocated to UAV m. Results are shown in Table II. Results are consistent with previous analysis, however, because robots maintain an altitude above the receiver array ground position as they travel, we expect some changes in performance, namely the degradation of capacity gains for the linear method.

TABLE II: Trial Times and Gains

| Case	$\Delta x(m)$	TDMA	Zero Δz (hr)	Fixed Δz (hr)	Linear Δz (hr)	Gain %
1D	50	2.172	2.116	1.704	1.086	36.27
	150	2.196	1.455	1.676	1.109	23.78
	300	2.232	1.273	1.689	1.163	8.64
	450	2.266	1.307	1.739	1.356	-3.75
2D	50	11.415	15.695	11.351	6.521	42.55
	150	3.806	3.380	3.764	2.456	27.34
	300	2.208	1.670	1.935	1.644	1.56
	450	1.681	1.228	1.340	1.351	-10.02

In Table II gain values listed are computed gain $= \frac{T_a - T_l}{T_a} \times 100$. The linear Δz method is denoted by subscript l versus lowest alternative method a.

2) 2D Path Planning: The same four Δz constraints from 1D planning are used to compute solutions to boustrophedon complete coverage flight plans. A sensing ROI consists of all waypoints defining the zero Δz method. If a z-offset occurs between robots, one robot will travel outside the ROI. An example of a boustrophedon for the linear Δz method is shown in Fig. 6b. Similar to 1D planning, this research assumes path plan augmentation can be accommodated. We choose a region where the upper bound of R_z is kept proportionally low, from previous analysis we expect the linear method to be effective. Table II demonstrates the ROI generates large performance gains by the linear method when inter-robot spacing is lower. Given transmitter travel of $[1, 3]$ km in the x-direction is not large, performance loss by increasing Δx is pronounced.

B. Evaluation under realistic conditions

To determine how MIMO SM methods perform under realistic conditions, the channel was simulated using ray tracing software [40]. The ray tracing simulation accounts for reflected paths due to the environment in addition to LOS. A dataset was generated for an urban environment in the city of Ottowa shown in Fig. 5. The transmitters and receivers were placed on a plane at a height of 60 meters, above all buildings. This setup emulates a base station placed on a tower receiving data from UAVs. The channel was simulated using a grid of transmitters spanning the city with a separation of 10 m communicating to two receivers 1 m apart located 320 meters west of origin. Capacity was then calculated according to (2) as 2 transmitters were positioned at points on the grid.

Data from trials for varying separation values between transmitters is shown in Table III. The fixed $\Delta z = 30$ m for all trials. Realistic channel properties result in lower channel magnitudes and higher mission completion times. For the 25 m case, the fixed method proved best by a wide margin. A 30
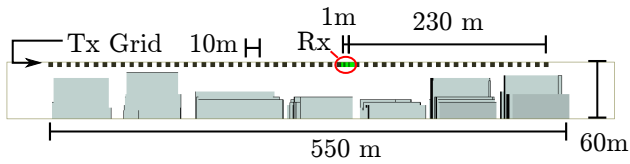
(a) South view of simulation environment. Transmitters and receivers are on the same plane at a height of 60 m above all buildings. The transmitters were simulated on a grid with separation of 10 m, while the receivers have a separation of 1 m.
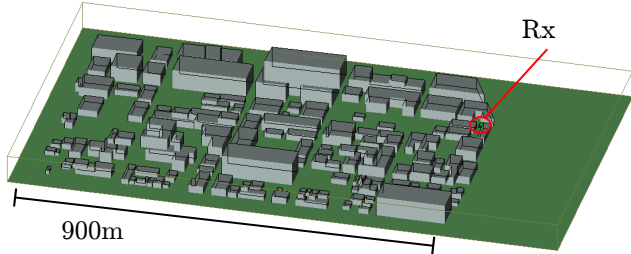
(b) South-east view of the environment showing the simulated city.

Fig. 5: The ray tracing simulation was performed in an urban environment spanning 550 m × 900 m. The simulated channel accounts for reflections occurring due to buildings along with the LOS path.

TABLE III: Trial Times and Gains

| $\Delta x(m)$	TDMA	Zero Δz (hr)	Fixed Δz (hr)	Linear Δz (hr)	Gain %
12.5	33.31	43.57	30.52	29.95	1.87
25	15.56	19.63	12.75	16.41	-28.71
50	9.16	13.73	7.87	6.94	11.82
100	5.35	7.00	5.32	3.74	29.70

m separation fared the best for conditions, but it is difficult to apply intuition to achieve these results. Capacity for the case of $\Delta x = 100$ m is shown in Fig. 6a. We see in this plot the same trends for the capacity of the linear Δz method, where performance gains are highest as R increases. We also see an increase in relative performance as Δx increases. This may be due to the minimized trade-off of fewer instances when robots must travel outside the ROI, and less lateral travel in the z-direction.

The path plan for the case where the distance between boustrophedon rows, Δx, is equal to 50 m is shown in Fig. 6b. The robots begin at $z = 0$ and move in a back and forth "lawnmower" motion. The boxes indicate an assumed sensing field of view. The dotted lines show the robot trajectories, where it is assumed robots are not imaging as they travel from one boustrophedon row to the next. The dashed black rectangle is the ROI, spanning 775 m in the x-direction and 350 m in the z-direction. It is assumed all robots with nonzero Δz offset were continuously imaging, thus their velocity was throttled even when travel outside of the ROI occurred.
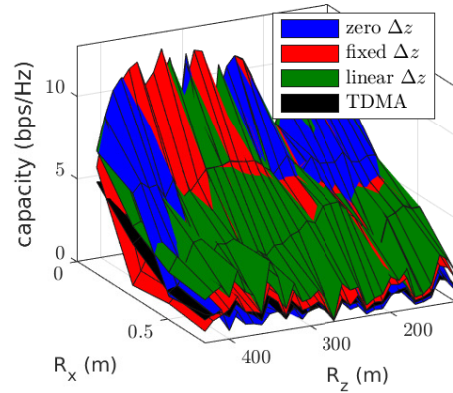
(a) Capacity is calculated using a ray tracing simulation of city conditions for a boustrophedon path plan with $\Delta x = 100$.
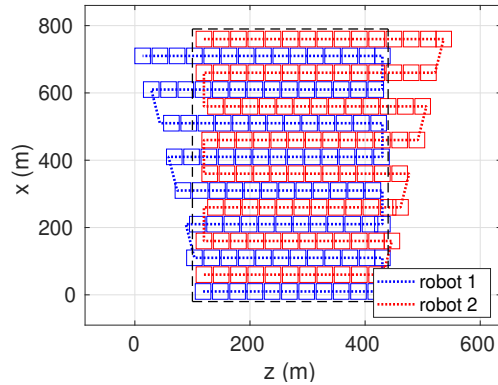
(b) The two robots move in a boustrophedon with a row separation of 50 m. The dashed black rectangle is the sensing ROI, all methods cover this region. In the linear Δz method shown, robots increasingly travel outside the ROI as they travel away from receivers.

Fig. 6: A capacity map corresponding to $\Delta x = 100$ m and a boustrophedon map corresponding to $\Delta x = 50$ m. The linear Δz method boustrophedon shown is one of 4 MIMO approaches to coverage planning in a realistic city environment.

V. CONCLUSIONS

In this work we analyze the benefit of SM methods for MIMO network enhancement in data aggregation tasks. By characterizing the capacity within a workspace we identify trends impacting communications throughput for a path following and coverage task. Based on this analysis we identify regions where ULA heuristics for static array design can improve capacity in a mobile sensing task. We validate our approach via simulations using both analytical and realistic approaches. In the future we plan account for motion in the z-direction of travel [16], [17]. This will add complexity because changes in Δz will result from displacements in all directions of travel. This extension allows for inclusion of more sophisticated sensing tasks while still achieving optimized communication.

REFERENCES

[1] M. A. Hsieh, A. Cowley, J. F. Keller, L. Chaimowicz, B. Grocholsky, V. Kumar, C. J. Taylor, Y. Endo, R. C. Arkin, B. Jung, D. F. Wolf, G. S.

Sukhatme, and D. C. MacKenzie, "Adaptive teams of autonomous aerial and ground robots for situational awareness: Field reports," *J. Field Robot.*, vol. 24, no. 11-12, pp. 991–1014, Nov. 2007.

[2] Y. Kantaros and M. M. Zavlanos, "Distributed Intermittent Connectivity Control of Mobile Robot Networks," *IEEE Transactions on Automatic Control*, vol. 62, no. 7, pp. 3109–3121, Jul. 2017.

[3] A. Muralidharan and Y. Mostofi, "Path Planning for Minimizing the Expected Cost until Success," *arXiv:1802.00898 [cs]*, Aug. 2018, arXiv: 1802.00898.

[4] U. Ali, H. Cai, Y. Mostofi, and Y. Wardi, "Motion-Communication Co-Optimization With Cooperative Load Transfer in Mobile Robotics: An Optimal Control Perspective," *IEEE Transactions on Control of Network Systems*, vol. 6, no. 2, pp. 621–632, Jun. 2019.

[5] Yuan Yan and Y. Mostofi, "Communication and path planning strategies of a robotic coverage operation," in *2013 American Control Conference*. Washington, DC: IEEE, Jun. 2013, pp. 860–866.

[6] A. Muralidharan and Y. Mostofi, "Path Planning for a Connectivity Seeking Robot," in *2017 IEEE Globecom Workshops (GC Wkshps)*. Singapore: IEEE, Dec. 2017, pp. 1–6.

[7] A. Muralidharan and Y. Mostofi, "Distributed beamforming using mobile robots," in *2016 IEEE International Conference on Acoustics, Speech and Signal Processing (ICASSP)*, March 2016, pp. 6385–6389.

[8] ——, "Energy optimal distributed beamforming using unmanned vehicles," vol. 5, no. 4, 2018, pp. 1529–1540.

[9] A. Ghaffarkhah and Y. Mostofi, "Path planning for networked robotic surveillance," *IEEE Transactions on Signal Processing*, vol. 60, no. 7, pp. 3560–3575, July 2012.

[10] S. Hayat, E. Yanmaz, T. X. Brown, and C. Bettstetter, "Multi-objective UAV path planning for search and rescue," in *2017 IEEE International Conference on Robotics and Automation (ICRA)*, May 2017, pp. 5569–5574, iSSN: null.

[11] A. Goldsmith, *Wireless Communications*. USA: Cambridge University Press, 2005.

[12] A. J. Paulraj, D. A. Gore, R. U. Nabar, and H. Bolcskei, "An overview of MIMO communications - a key to gigabit wireless," *Proceedings of the IEEE*, vol. 92, no. 2, pp. 198–218, Feb 2004.

[13] D. Tse and P. Viswanath, *Fundamentals of wireless communication*. Cambridge university press, 2005.

[14] T. Haustein and U. Kruger, "Smart geometrical antenna design exploiting the LOS component to enhance a MIMO system based on rayleigh-fading in indoor scenarios," in *14th IEEE Proceedings on Personal, Indoor and Mobile Radio Communications, 2003. PIMRC 2003.*, vol. 2. Beijing, China: IEEE, 2003, pp. 1144–1148.

[15] D. Gesbert, H. Bolcskei, D. Gore, and A. Paulraj, "Outdoor MIMO wireless channels: models and performance prediction," *IEEE Transactions on Communications*, vol. 50, no. 12, pp. 1926–1934, Dec. 2002.

[16] F. Bohagen, P. Orten, and G. E. Oien, "Design of Optimal High-Rank Line-of-Sight MIMO Channels," *IEEE Transactions on Wireless Communications*, vol. 6, no. 4, pp. 1420–1425, Apr. 2007.

[17] F. Bohagen, P. Orten, and G. Oien, "Optimal Design of Uniform Rectangular Antenna Arrays for Strong Line-of-sight MIMO Channels," *EURASIP J. Wirel. Commun. Netw.*, vol. 2007, no. 2, pp. 12–12, Jan. 2007.

[18] S. Hanna, H. Yan, and D. Cabric, "Distributed uav placement optimization for cooperative line-of-sight mimo communications," in *ICASSP 2019 - 2019 IEEE International Conference on Acoustics, Speech and Signal Processing (ICASSP)*, May 2019, pp. 4619–4623.

[19] N. Chatzipanagiotis, Y. Liu, A. Petropulu, and M. M. Zavlanos, "Controlling groups of mobile beamformers," in *2012 IEEE 51st IEEE Conference on Decision and Control (CDC)*, Dec. 2012, pp. 1984–1989.

[20] S. Hanna, E. Krijestorac, H. Yan, and D. Cabric, "UAV Swarms as Amplify-and-Forward MIMO Relays," in *2019 IEEE 20th International Workshop on Signal Processing Advances in Wireless Communications (SPAWC)*, Jul. 2019, pp. 1–5.

[21] W. Du, W. Ying, P. Yang, X. Cao, G. Yan, K. Tang, and D. Wu, "Network-Based Heterogeneous Particle Swarm Optimization and Its Application in UAV Communication Coverage," *IEEE Transactions on Emerging Topics in Computational Intelligence*, pp. 1–12, 2019, citation Key Alias: du_network-based_2019-1.

[22] T. Cabreira, L. Brisolara, and P. R. Ferreira Jr., "Survey on Coverage Path Planning with Unmanned Aerial Vehicles," *Drones*, vol. 3, no. 1, p. 4, Jan. 2019.

[23] E. Galceran and M. Carreras, "A survey on coverage path planning for robotics," *Robot. Auton. Syst.*, vol. 61, no. 12, p. 1258–1276, Dec. 2013.

[24] C. Deng, S. Wang, Z. Huang, Z. Tan, and J. Liu, "Unmanned Aerial Vehicles for Power Line Inspection: A Cooperative Way in Platforms and Communications," *Journal of Communications*, vol. 9, no. 9, pp. 687–692, 2014.

[25] "Automatic system for overhead power line inspection using an Unmanned Aerial Vehicle — RELIFO project," May 2013, pp. 244–252.

[26] Y. Zhang, X. Yuan, Y. Fang, and S. Chen, "UAV Low Altitude Photogrammetry for Power Line Inspection," EARTH SCIENCES, preprint, Aug. 2016.

[27] Y. Zhang, X. Yuan, W. Li, and S. Chen, "Automatic Power Line Inspection Using UAV Images," *Remote Sensing*, vol. 9, no. 8, p. 824, Aug. 2017.

[28] V. T. Hoang, M. D. Phung, T. H. Dinh, and Q. P. Ha, "Angle-Encoded Swarm Optimization for UAV Formation Path Planning," *2018 IEEE/RSJ International Conference on Intelligent Robots and Systems (IROS)*, pp. 5239–5244, Oct. 2018, arXiv: 1812.07873.

[29] V. T. Hoang, M. D. Phung, T. H. Dinh, and Q. Ha, "System architecture for real-time surface inspection using multiple uavs," 07 2019.

[30] L. Duque, "UAV-Based Bridge Inspection and Computational Simulations," Master's thesis, South Dakota State University, 2017.

[31] C.-H. Yang, M.-C. Wen, Y.-C. Chen, and S.-C. Kang, "An optimized unmanned aerial system for bridge inspection," in *ISARC. Proceedings of the International Symposium on Automation and Robotics in Construction*, vol. 32. IAARC Publications, 2015, p. 1.

[32] J. Seo, L. Duque, and J. Wacker, "Drone-enabled bridge inspection methodology and application," *Automation in Construction*, vol. 94, pp. 112–126, Oct. 2018.

[33] D. Hausamann, W. Zirnig, and G. Schreier, "Monitoring of Gas Transmission Pipelines – a Customer Driven Civil UAV Application," in *ODAS Conference*, 2003, p. 15.

[34] A. Shukla, H. Xiaoqian, and H. Karki, "Autonomous tracking of oil and gas pipelines by an unmanned aerial vehicle," in *2016 IEEE 59th International Midwest Symposium on Circuits and Systems (MWSCAS)*, Oct. 2016, pp. 1–4, iSSN: 1558-3899.

[35] L. I. Kochetkova, "Pipeline monitoring with unmanned aerial vehicles," *Journal of Physics: Conference Series*, vol. 1015, p. 042021, May 2018.

[36] S. Waharte and N. Trigoni, "Supporting Search and Rescue Operations with UAVs," in *2010 International Conference on Emerging Security Technologies*, Sep. 2010, pp. 142–147, iSSN: null.

[37] P. Cohn, A. Green, M. Langstaff, and M. Roller, "Commercial drones are here: The future of unmanned aerial systems," McKinsey & Company, Tech. Rep., 2018.

[38] A. Ahmadzadeh, J. Keller, G. Pappas, A. Jadbabaie, and V. Kumar, "An optimization-based approach to time-critical cooperative surveillance and coverage with uavs," in *Experimental Robotics*. Springer, 2008, pp. 491–500.

[39] S. Hayat, E. Yanmaz, and R. Muzaffar, "Survey on Unmanned Aerial Vehicle Networks for Civil Applications: A Communications Viewpoint," *IEEE Communications Surveys & Tutorials*, vol. 18, no. 4, pp. 2624–2661, 2016.

[40] Remcom, "Wireless EM Propagation Software - Wireless InSite," https://www.remcom.com/wireless-insite-em-propagation-software.